The Role of Linear Interference in the Annular Mode Response to Tropical SST Forcing

CHRISTOPHER G. FLETCHER AND PAUL J. KUSHNER

Department of Physics, University of Toronto, Toronto, Ontario, Canada

(Manuscript received 18 March 2010, in final form 8 September 2010)

ABSTRACT

Recent observational and modeling studies have demonstrated a link between eastern tropical Pacific Ocean (TPO) warming associated with the El Niño–Southern Oscillation (ENSO) and the negative phase of the wintertime northern annular mode (NAM). The TPO–NAM link involves a Rossby wave teleconnection from the tropics to the extratropics, and an increase in polar stratospheric wave driving that in turn induces a negative NAM anomaly in the stratosphere and troposphere. Previous work further suggests that tropical Indian Ocean (TIO) warming is associated with a positive NAM anomaly, which is of opposite sign to the TPO case. The TIO case is, however, difficult to interpret because the TPO and TIO warmings are not independent. To better understand the dynamics of tropical influences on the NAM, the current study investigates the NAM response to imposed TPO and TIO warmings in a general circulation model. The NAM responses to the two warmings have opposite sign and can be of surprisingly similar amplitude even though the TIO forcing is relatively weak. It is shown that the sign and strength of the NAM response is often simply related to the phasing, and hence the linear interference, between the Rossby wave response and the climatological stationary wave. The TPO (TIO) wave response reinforces (attenuates) the climatological wave and therefore weakens (strengthens) the stratospheric jet and leads to a negative (positive) NAM response. In additional simulations, it is shown that decreasing the strength of the climatological stationary wave reduces the importance of linear interference and increases the importance of nonlinearity. This work demonstrates that the simulated extratropical annular mode response to climate forcings can depend sensitively on the amplitude and phase of the climatological stationary wave and the wave response.

1. Introduction

Tropical variability related to the El Niño–Southern Oscillation (ENSO) is associated with large-scale atmospheric teleconnections that influence seasonal weather and climate variability over much of the globe (e.g., Trenberth et al. 1998). Here, we focus on the connection between ENSO and the northern annular mode (NAM; Thompson and Wallace 2000), which is the dominant pattern of variability in the Northern Hemisphere extratropical circulation on intraseasonal and longer time scales. While a lack of sufficient data and sampling issues may have previously obscured such a link in observations (Free and Seidel 2009), a consensus is now emerging that warm ENSO events are associated with the negative polarity of the wintertime NAM (Brönnimann 2007; Garfinkel and Hartmann 2008; Manzini 2009). Several recent modeling studies have investigated the physical mechanisms of this link and highlight the important role played by wave–mean flow interactions in the polar stratosphere in setting up the NAM response in the stratosphere and troposphere (Ineson and Scaife 2009; Cagnazzo and Manzini 2009; Bell et al. 2009).

Recent work on the ENSO–NAM connection has pointed out the importance of the coherence of the ENSO-related planetary wave with the extratropical climatological stationary wave. The tropospheric Rossby wave anomaly associated with ENSO warming is well known to project onto the positive phase of the Pacific–North American (PNA) pattern (e.g., Horel and Wallace 1981). The ENSO-related wave is in phase with the climatological stationary wave over the North Pacific, and on a planetary scale has been shown to amplify the climatological zonal wavenumber 1 by 10%–20% during El Niño events (Ineson and Scaife 2009; Garfinkel and Hartmann 2008; Manzini et al. 2006). Wave 1 propagates into the stratosphere efficiently, by the Charney–Drazin

Corresponding author address: Christopher G. Fletcher, Dept. of Physics, University of Toronto, 60 St. George St., Toronto M5S 1A7, Canada.
E-mail: chris.fletcher@utoronto.ca

DOI: 10.1175/2010JCLI3735.1

theory, and is most important for stratospheric wave–mean flow interaction. The amplification of this wave increases planetary wave driving in the stratosphere and therefore tends to weaken the stratospheric polar vortex (Ineson and Scaife 2009; Garfinkel and Hartmann 2008), which is highly coherent with the NAM signature in the lower troposphere (Baldwin and Dunkerton 2001; Polvani and Waugh 2004).

Although the primary influence of ENSO on the NAM is thought to come from warm sea surface temperature (SST) anomalies in the tropical Pacific Ocean (TPO), there is indirect evidence that variability in the tropical Indian Ocean (TIO) may also be involved. Typically, the TIO warms 2–3 months after a warming in the eastern Pacific (Alexander et al. 2002), partly as a thermodynamic response to subsidence and suppressed convection associated with ENSO and partly as a dynamical response caused by changes to surface wind stresses. The thermodynamic part involves the atmosphere driving the ocean, whereas the dynamical part induces its own weaker forcing on the atmosphere through convective heating. The extratropical impacts of this additional heating have been considered in a few studies (Hoerling et al. 2004; Annamalai et al. 2007). For example, Hoerling et al. (2004) showed that imposed SST warming in the tropical Indian Ocean was associated with the positive phase North Atlantic Oscillation (NAO). Since the NAO and NAM are highly correlated, Hoerling et al.'s analysis suggests that externally forced Indian Ocean warming leads to a positive NAM signal.

Our main interest in this study is to understand the separate impacts of TIO and TPO warmings on the NAM, which represents a primary measure of the extratropical zonal mean circulation of the stratosphere and troposphere. It is already well known that imposed warmings in different tropical locations yield very different extratropical wave teleconnections (e.g., Branstator and Haupt 1998; Barsugli and Sardeshmukh 2002; Annamalai et al. 2007). For example, Annamalai et al. (2007) found opposite-signed extratropical teleconnections in two sets of experiments forced by TPO and TIO SST anomalies. There appears to be a nodal line in tropical SST around 100°E about which the sensitivity of the extratropical response changes sign (Barsugli and Sardeshmukh 2002). However, to our knowledge no equivalent sensitivity analysis has been performed for the extratropical zonal mean/NAM response to tropical SST forcing. The existing literature suggests the hypothesis that imposed TPO warming will force a negative NAM signal, while imposed TIO warming will force a positive NAM signal. This hypothesis is somewhat surprising because there is no obvious reason why a change in location of the warming would yield an opposite-signed zonal mean response. In section 3a of this study, we will show simulations using a comprehensive GCM that confirm this hypothesis. To explain these results dynamically, we will show (sections 3b and 3c) that constructive interference or destructive interference between the forced wave and the climatological wave controls the sign and amplitude of the wave-driven NAM response in the stratosphere and troposphere. In recent work, we have shown that similar interference effects also operate in the NAM response to extratropical surface thermal forcing (Smith et al. 2010).

The relevance of our findings to observations is complicated by the well-known problems associated with imposing SST anomalies as external forcings in an atmospheric GCM (e.g., Wu et al. 2006). Generally, if a particular region of SST anomaly represents a response to a remote forcing, the dynamical atmospheric response might not be well captured by imposing that SST anomaly as a boundary perturbation. We alluded to this issue in discussing the causes of Indian Ocean warming. Despite these complications, we find there is much insight to be gained about the extratropical zonal mean response problem by considering the effects of TPO and TIO forcing separately and together. The results of this study will be directly applicable to prescribed SST simulations of the Atmospheric Model Intercomparison Project (AMIP) type, and more indirectly applicable to observations, as long as they are properly interpreted.

We next describe our modeling methodology (section 2) and present the results from our simulations (section 3). Section 4 provides conclusions and a discussion.

2. Model and methods

a. GFDL AM2 model

All model simulations are performed using the Geophysical Fluid Dynamics Laboratory (GFDL) Global Atmosphere and Land Models (AM2–LM2; Anderson et al. 2004). This version has a finite-volume dynamical core (Lin 1994) and forms the atmospheric component of the Coupled Ocean–Atmosphere Model (CM2.1) used in the Intergovernmental Panel on Climate Change (IPCC) Fourth Assessment Report (Delworth et al. 2006). The horizontal resolution is 2° latitude × 2.5° longitude and there are 24 vertical layers with a model lid at 3 hPa (~50 km). This model does not have a well-resolved stratosphere, which might affect the overall amplitude of the NAM response to tropical forcing (Cagnazzo and Manzini 2009). On the other hand, the model has several advantages: 1) it has been shown to represent well ENSO-related tropical precipitation and extratropical teleconnection patterns (Anderson et al. 2004); 2) it carries relatively low computational cost

TABLE 1. List of SST perturbation experiments analyzed in this study. All SST fields are derived from a global composite of HadISST (Rayner et al. 2003) computed for the five warmest El Niño years (DJF) during 1950–2001 (see Fig. 1 and section 2b). The second column (N) specifies the number of independent realizations performed for each experiment.

Expt	N	Description of SST perturbation
TPO	100	Warming anomalies associated with El Niño events imposed in the tropical Pacific (15°S–15°N, 172°–75°E)
TIO	100	As in TPO but for warming anomalies in the tropical Indian Ocean (30°S–30°N, 40°–120°E)
TIP	50	TPO and TIO warming anomalies imposed together
TPO_{NOTIB}	100	As in TPO but with reduced topography over Tibet and eastern Eurasia
TIO_{NOTIB}	50	As in TIO but with reduced topography over Tibet and eastern Eurasia
TPO_{NOROCK}	50	As in TPO but with reduced topography over the Rockies
TPO × 1.5	50	As in TPO but with SST warming anomalies multiplied by a factor of 1.5
TPO × 0.5	50	As in TPO but with SST warming anomalies multiplied by a factor of 0.5
TIP±	30	As in TIP but for warming and cooling anomalies imposed across the entire TIP region (30°S–30°N, 40°–75°E)
TOGA	30	As in TIP but for warming and cooling anomalies imposed throughout the tropics (30°S–30°N, 0°–359°E)
GOGA	30	As in TIP but for warming and cooling anomalies imposed globally (60°S–60°N, 0°–359°E)

compared to a model with a well-resolved stratosphere, which allows us to carry out several hundred seasonal timescale realizations; 3) it is one of the primary models used in current work on climate assessment and seasonal prediction; and 4) it produces results related to stratosphere–troposphere coupling that are qualitatively consistent with a similar model with greater stratospheric resolution (Fletcher et al. 2009). Most importantly, our main interest is in understanding the dynamics of the sensitivity of the NAM response to different forcings, and this model produces NAM responses that are consistent with expectations from the literature cited in section 1.

We investigate the extratropical atmospheric response to switch-on tropical SST perturbations during the December–February (DJF) period. To ensure a high signal-to-noise ratio in the extratropics, we generate large ensembles of independent realizations of the same simulation (see Table 1). This is achieved by first running a 100-yr control simulation with atmospheric composition fixed at 1990 levels and a climatological seasonal cycle of sea surface temperatures and sea ice. We take each 1 December restart file from this control simulation and branch a new 3-month (DJF) perturbation simulation with the time-independent SST perturbation applied. Thus, every realization of the perturbation or control simulation shares the same lower boundary forcing but, assuming independence from year to year in the control simulation, has independent initial conditions. The response to the forcing is the ensemble mean difference between the 100 pairs of perturbed and control simulations. For all figures shown, following the approach of Annamalai et al. (2007) the first month (December) of the integrations is discarded, and we present the January–February (JF) mean. This is to remove the influence of any initial rapid adjustment to the switch-on perturbation. We have verified that this does not qualitatively change the results presented (not shown).

b. SST perturbations

The simulations we use are described in Table 1. We focus primarily on the response to the SST anomalies shown in Fig. 1a, which plots the SST warming perturbations associated with the warm phase of ENSO for the TPO and the TIO. The nomenclature and approach are similar to Annamalai et al. (2007). The patterns are constructed as follows. First, we produce a composite of the five warmest DJF El Niño episodes during 1950–2001 from the Hadley Centre Global Sea Ice Coverage and Sea Surface Temperature dataset (HadISST) observational reconstruction (Rayner et al. 2003). The global SST anomaly patterns from the composite are shown in Fig. 1b. From this global composite we extract only the warm (positive) SST anomalies from the TPO region (15°S–15°N, 172°–285°E) and the TIO region (30°S–30°N, 40°–120°E). All anomalies outside of the TIO and TPO regions are set to zero. In addition, unlike Annamalai et al. (2007), the negative anomalies within the forcing region are set to zero so that we can examine only the response to SST warming, in a manner similar to Barsugli et al. (2006). The appropriate perturbation pattern is then added to the seasonally varying monthly mean climatological SST field to produce the model forcing field for each simulation. Note that the area-integrated amplitude of the TIO SST forcing is only 30% of that in TPO.

As in Annamalai et al. (2007), we also conduct perturbation simulations where the TPO and TIO forcings are imposed together (denoted tropical Indo-Pacific or TIP). Table 1 also lists a series of additional simulations conducted to examine the sensitivity of our results, and the degree to which they apply more generally: (a) TIP±, where the full SST anomaly field associated with the El Niño composite described above, including both warm and cold anomalies, is imposed throughout the TIP region; (b) TOGA (for Tropical Ocean Global

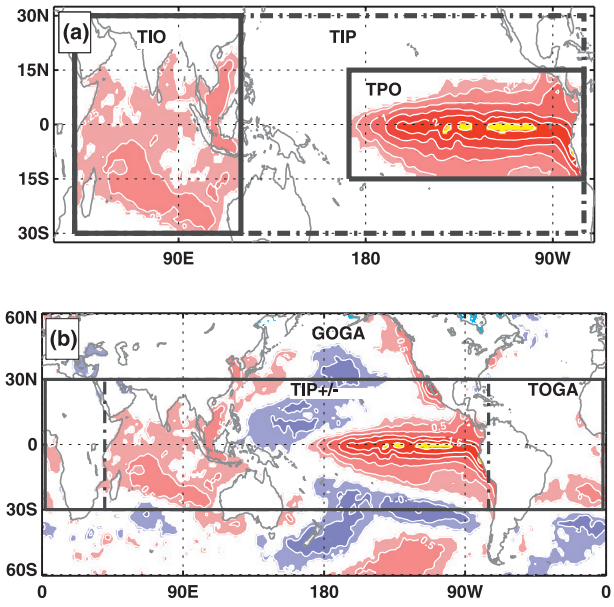

FIG. 1. (a) The positive (warming) SST anomalies (contours and shading) imposed in the TIO, TPO, and TIP experiments, which are derived from the full composite of global (60°S–60°N) SST anomalies from HadISST (Rayner et al. 2003) for the five warmest El Niño events during 1950–2001. The contour and shading interval are ±0.25 K, ±0.5 K, and then the interval is ±0.5 K. Anomalies in the entire region in (b) were imposed for the GOGA experiment (Table 1), the solid box shows the TOGA region, and the dashed box shows the TIP ± subregion.

Atmosphere), which is the same as TIP± except the SST anomalies are imposed throughout the entire tropics; (c) GOGA, which is the same as TOGA except the SST anomalies are imposed globally; (d) TPO × 0.5 and TPO × 1.5, in which the warm SST anomalies in TPO are multiplied by factors of 0.5 and 1.5 to test the sensitivity of the response to changes in forcing strength; and (e) a series of simulations forced by TPO and TIO SST anomalies that include reduced topography over Tibet and eastern Eurasia (NOTIB) and over the Rockies (NOROCK), where we examine how tropical–extratropical teleconnections change when the climatological stationary waves are weakened (see section 3d). The GOGA, TOGA, and associated SST regions are shown in Fig. 1b.

Finally, the statistical significance is computed for all figures using the Student's t test for the difference of means (Wilks 2006). The large number of realizations in our ensemble ensures a high level of robustness in the response; all features discussed below are significantly different from zero with $p < 0.05$, even in the simulations with fewer realizations (Table 1). Therefore, to simplify our figures, we have not included any significance shading.

3. Results

a. Tropical–extratropical response

In the TIP, TPO, and TIO simulations, the imposed tropical SST warming triggers a deep convective response in the vicinity of the forcing, collocated areas of upper-tropospheric divergence, and areas of convergence and subsidence to the west and east. These features are shown in Fig. 2 and agree with several previous GCM studies (e.g., Kumar and Hoerling 1998, Annamalai et al. 2007).[1] The TIP (Fig. 2a) and TPO (Fig. 2b) responses are very similar over the tropical Pacific, but they are very different over the tropical Indian Ocean, and the TIO response is more localized than the TPO response. The different spatial scales of the TIO and TPO responses are reflected in the extratropical wave responses, as we will discuss below.

To check for linear additivity, we compare the sum of the TIO and TPO responses in Fig. 2d to the TIP response in Fig. 2a. The responses are generally additive, especially over the Pacific, where the TIO forcing appears to have little remote influence. Over the Indian Ocean, linear additivity is less well satisfied: for example, in the region centered on 5°S, 90°E, the convergence response in TIP is weaker than the sum of the TIO and TPO responses by around 50%. We will return to the issue of nonlinearity in the wave response to a wide variety of forcings and climatological regimes. Nevertheless, we can partially attribute the relatively weak response over the western Indian Ocean to cancellation between the TIO response (Fig. 2c), which is characterized by upwelling and divergence there, and the TPO response (Fig. 2b), which is characterized by downwelling and convergence there.

The convective response illustrated in Fig. 2 generates an extratropical Rossby wave that relates to our primary focus. Figure 3 shows that the Northern Hemisphere wave geopotential height responses for the TIP, TPO, and TIO cases all have similar wavelengths. As mentioned in section 2b, the TIO forcing has 30% of the amplitude of the TPO forcing; however, the area-integrated wave response in TIO has 55% of the amplitude of the TPO response, meaning the TIO forcing is a more efficient wave driver than the TPO forcing. The responses also have distinct propagation paths: the primary TIP and TPO wave trains refract equatorward while the primary TIO wave train propagates directly poleward. In agreement with many previous studies, the upper-tropospheric wave response to the TIP and TPO perturbations (Figs. 3a and 3b) projects strongly onto the positive phase of the

[1] The westward extension of the circulation response is predicted by classical theory (Gill 1980).

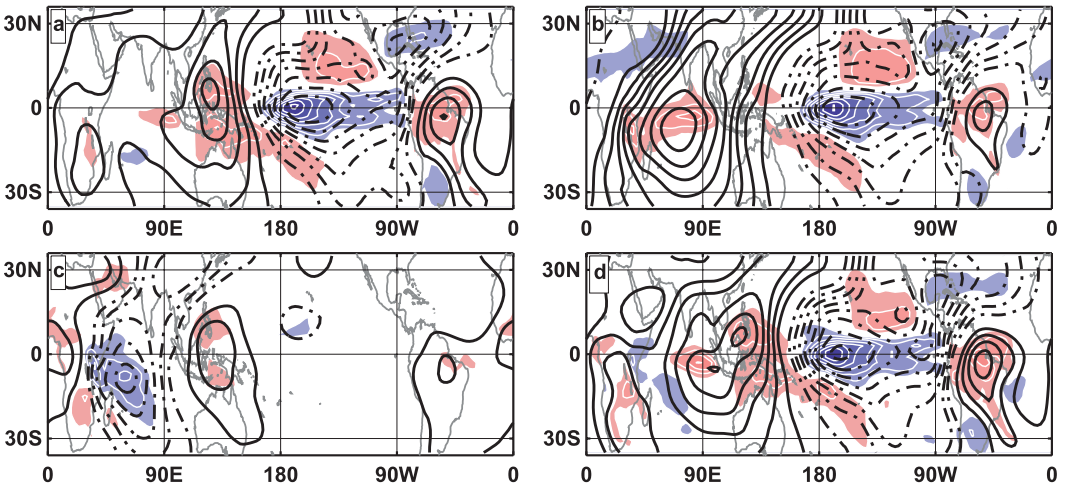

FIG. 2. The ensemble-mean JF time-averaged responses (perturbed − control) to (a) TIP, (b) TPO, and (c) TIO forcings. Shading and white contours show the outgoing longwave radiation response (interval 10 W m^{-2}). Black contours show the 200-hPa velocity potential response, with dashed contours indicating negative values (interval 5×10^5 m^2 s^{-1}). (d) Sum of the TPO and TIO responses.

Pacific–North American teleconnection pattern (Wallace and Gutzler 1981), with a deepened Aleutian low and an intensified high centered over the Canadian Arctic. Over the North Pacific sector the TIO response shows a high (indicative of a weakened Aleutian low) and projects onto the negative phase of the PNA. This is opposite to TPO and agrees with the results of Hoerling et al. (2004) and Annamalai et al. (2007). We also note that there is a weak North Atlantic sector response in the wave geopotential field that projects onto the positive phase of the North Atlantic Oscillation for both cases.

For wave-driven zonal mean NAM dynamics in which the stratosphere is implicated, the largest-scale waves play a controlling role. Accordingly in Fig. 4, we decompose the wave geopotential response into its wave-1 and -2 components. The wave-1 and -2 responses are approximately additive in the forcing: the sum of the TIO and TPO wave-1 (wave 2) responses explains 83% (73%) of the area-integrated TIP response. For wave 1, the TIO and TPO responses have a similar pattern but opposite sign, which reflects the fact that the forcing and wave responses are shifted by 180°. For wave 2, the TIO and TPO responses overall reinforce each other, which is reflected in the TIP wave-2 field's relatively strong amplitude.

Our main interest in this study is the zonal mean extratropical circulation response to tropical forcing. In Figs. 5a–c we show the Northern Hemisphere zonal mean geopotential height response [ΔZ] in the TIP, TPO, and TIO cases. We recall (Cohen et al. 2002; Baldwin and Thompson 2009) that [ΔZ] averaged poleward of 60°N is a proxy for the negative of the NAM in the troposphere and stratosphere. The TIP response consists of a positive geopotential response in the polar troposphere and stratosphere and corresponds to a negative NAM response (i.e., weak polar stratospheric vortex, positive polar cap heights). The TPO response is of the same sign and structure but has about 4–5 times the amplitude of the TIP response. The TIO response is of a similar magnitude to the TPO response but is of opposite sign, and thus corresponds to a positive NAM response (strong polar stratospheric vortex, negative polar cap heights). The sum of the TPO and TIO responses (Fig. 5d) explains the basic features of the weak TIP response (Fig. 5a). Although we will see below that not all aspects of the responses are similarly additive in the forcings, we can describe the relatively weak negative NAM response to TIP forcing in terms of a cancellation between a very strong negative NAM response from TPO and a somewhat weaker positive NAM response from TIO.

The positive NAM response in TIO is surprisingly strong despite the weak forcing: over the polar cap poleward of 60°N, the TIO response is about 80% of the strength of the TPO response, but as stated previously the TIO forcing strength (Fig. 1) and the wave response (Figs. 3 and 4) are 30% and 55% of the magnitude of TPO, respectively. This suggests that per unit SST warming, the Indian Ocean forcing is more than twice as efficient as the Pacific Ocean forcing at driving zonal mean changes at high latitudes. The similar strength and opposite sign of the TIO and TPO NAM responses is key to understanding the relatively weak TIP response in this model. We will show in sections 3b and 3c

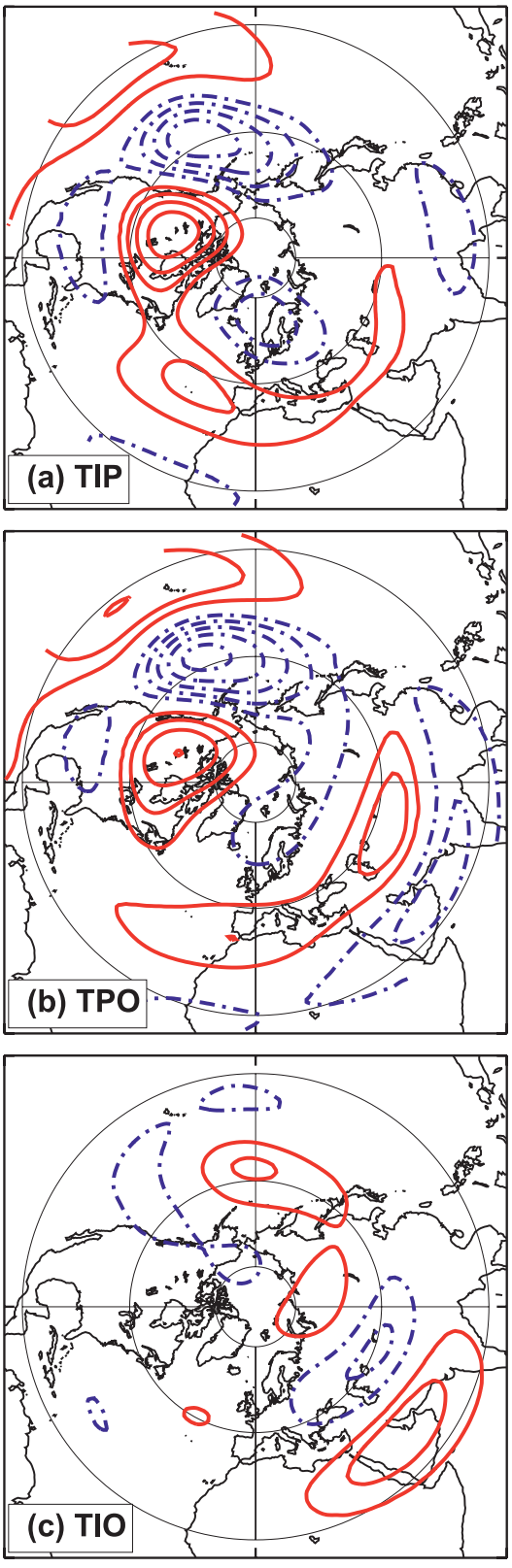

FIG. 3. The ensemble-mean JF response in 200-hPa wave geopotential height. Contour interval is 20 m and negative contours are dashed.

that the relative efficiency of TIO and TPO is related to the planetary wave driving of the zonal mean flow response.

In contrast, in the tropics the extratropical zonal mean geopotential response [ΔZ] has the same sign in all three simulations and scales roughly with forcing strength (Figs. 5a–c). On the basis of additional simulations, we will argue in section 3d that the tropical–subtropical zonal mean geopotential response is driven by the upper-tropospheric heating rather than being related to the wave-driven response.

In the remainder of this article we will focus on explaining the dynamics of the NAM response. We need to address what causes the NAM response to be of opposite sign and roughly equal magnitude when the forcing in the TIO case is only 30% of that in the TPO case. To address these questions, we must better understand the dynamical differences between the high-latitude responses in TPO and TIO, and determine how the waves produced by each perturbation (Figs. 3 and 4) affect the zonal mean flow (Fig. 5).

b. *Wave-activity flux decomposition*

The wave-driven zonal response is related to the response of the Eliassen–Palm (EP) flux, which is quadratic in wave amplitude. In this section we develop a decomposition of the EP flux response that has proven useful in diagnosing the wave-driven response in these simulations.

In the stratosphere the EP flux and its divergence are dominated by the vertical component that is approximately proportional to the zonal mean meridional flux of sensible heat by the eddies (Newman et al. 2001). We call this quantity $\{v^*T^*\}$, where the braces $\{\cdots\}$ denote zonal and time averaging, and the star denotes a departure from the zonal mean. We decompose $\{v^*T^*\}$ and its response into three distinct terms. The following decomposition, introduced in Smith et al. (2010), is illustrated for $\{v^*T^*\}$ with the understanding that it applies to all the terms in the EP flux. This decomposition is the basis for Fig. 6, which presents our key results.

For each realization in the ensemble, we have

$$v^* = \langle v^* \rangle + v^{*\prime}, T^* = \langle T^* \rangle + T^{*\prime},$$

where the angle brackets denote an ensemble mean and the prime a departure from the ensemble mean. The ensemble mean response of the wave activity flux, $\Delta\{v^*T^*\}$, is decomposed as

$$\Delta\{\langle v^*T^*\rangle\} = \Delta\{\langle v^*\rangle\langle T^*\rangle\} + \Delta\{\langle v^{*'}T^{*'}\rangle\}. \quad (1)$$

The first term on the r.h.s. of (1) is the heat flux response associated with the ensemble mean eddy response, while

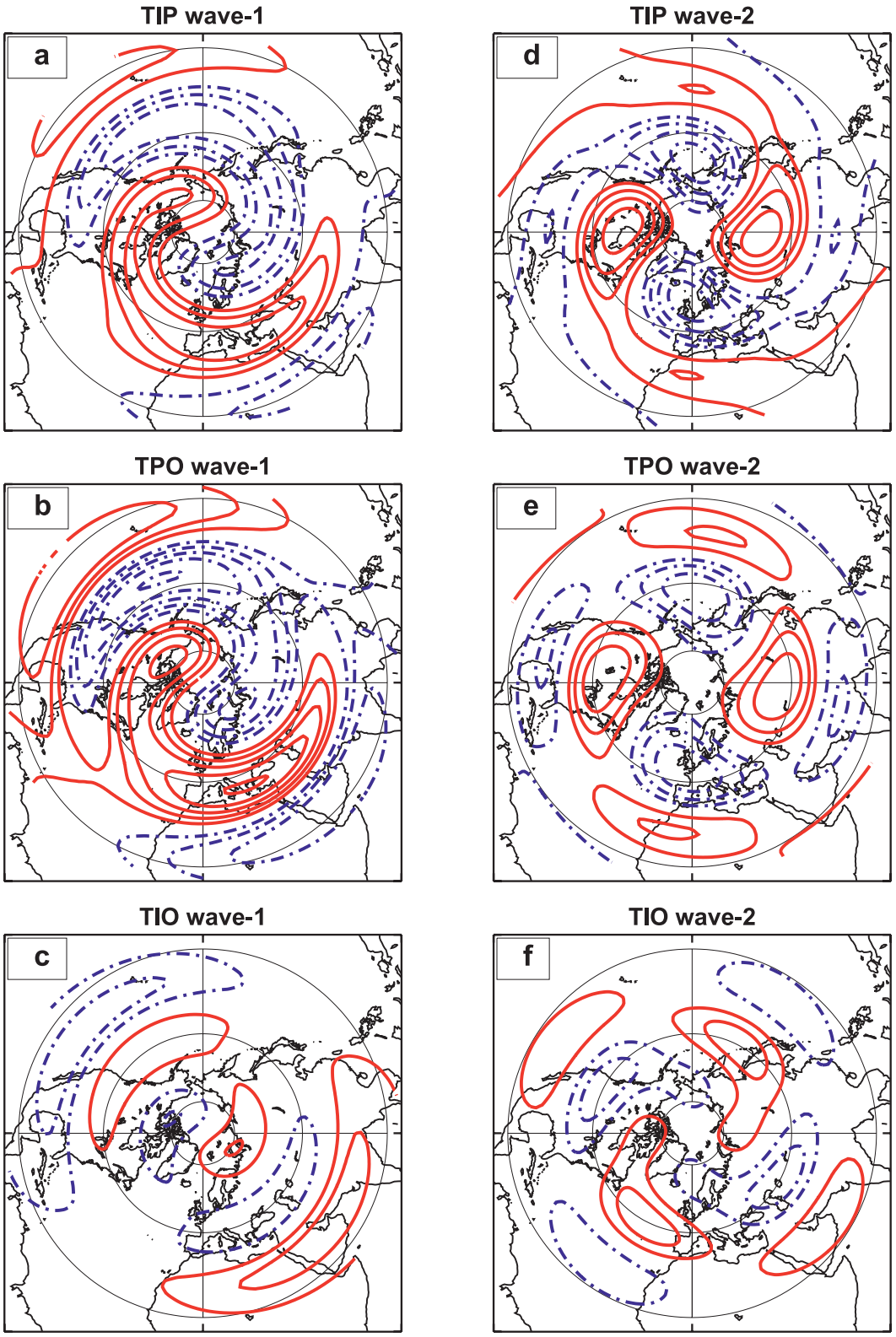

FIG. 4. As in Fig. 3, but the left-hand (right-hand) panels show the zonal wave-1 (wave 2) component of the 200-hPa wave geopotential height response. Contour interval is 10 m and negative contours are dashed.

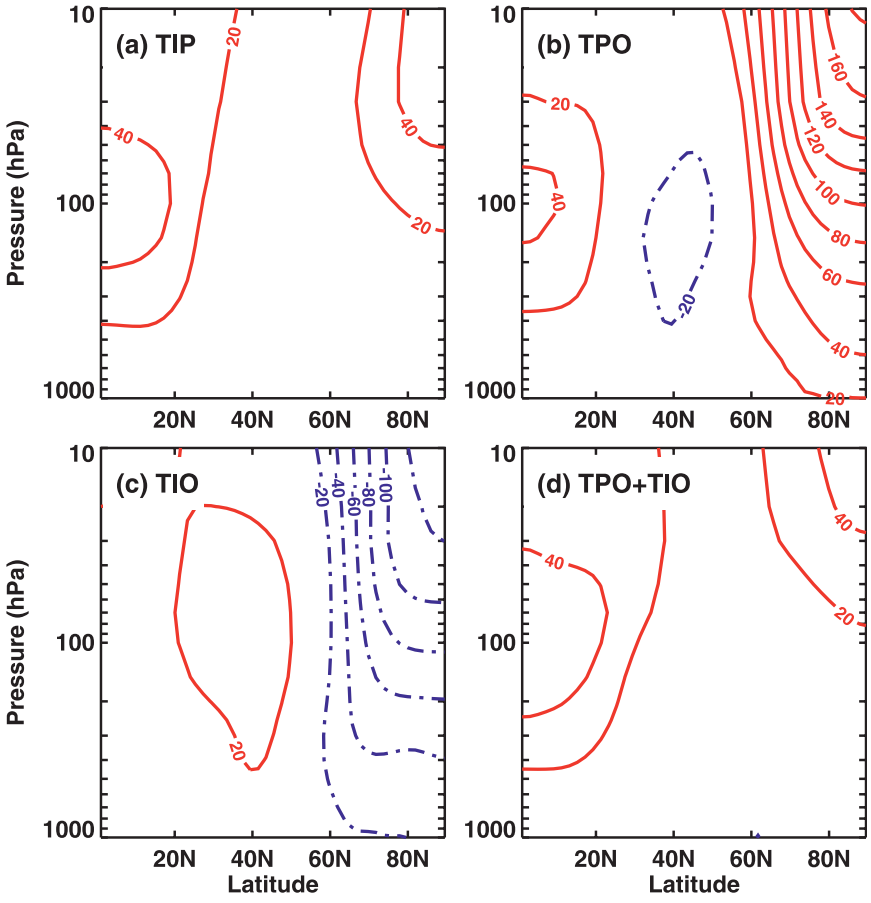

FIG. 5. The ensemble-mean JF zonal mean geopotential height response as a function of latitude and pressure in (a) TIP, (b) TPO, (c) TIO, and (d) the sum of the TPO and TIO responses. The contour interval is 20 m and negative contours are dashed.

the second term is the heat flux response associated with departures from the ensemble mean. The second term characterizes higher-frequency variability than the first term because ensemble averaging effectively acts as a low-pass filter on the fields. For example, we find (not shown) that in the troposphere the second term includes synoptic waves that are randomly phased from one realization to the next but that systematically transport heat poleward in the troposphere, leading to a positive term $\{\langle v^{*\prime} T^{*\prime}\rangle\}$. We call the first term in (1) EM, which is the heat flux response associated with the ensemble mean wave, and the second term in (1) FL, which is the heat flux response associated with the fluctuations about the ensemble mean. We can then write

$$\Delta\{\langle v^* T^*\rangle\} = \text{TOTAL} = \text{EM} + \text{FL}, \tag{2}$$

where

$$\text{EM} \equiv \Delta\{\langle v^*\rangle\langle T^*\rangle\} \quad \text{and} \quad \text{FL} \equiv \Delta\{\langle v^{*\prime} T^{*\prime}\rangle\}. \tag{3}$$

The EM term can be further decomposed as follows. First, we decompose the ensemble mean response in each field as

$$\langle v^*\rangle = v_c + \Delta\langle v^*\rangle, \langle T^*\rangle = T_c + \Delta\langle T^*\rangle,$$

where the subscript c refers to the background (climatological, i.e., 100-yr average) stationary wave from the unforced control simulation. Then,

$$\text{EM} = \text{EM}_{\text{LIN}} + \text{EM}_{\text{NL}}, \tag{4}$$

where

$$\text{EM}_{\text{LIN}} \equiv \{v_c^* \Delta\langle T^*\rangle\} + \{\Delta\langle v^*\rangle T_c^*\} \quad \text{and}$$
$$\text{EM}_{\text{NL}} \equiv \{\Delta\langle v^*\rangle \Delta\langle T^*\rangle\}. \tag{5}$$

In (2)–(5), we emphasize that the zonal and time average is being taken on each product term.

In (4) and (5), the term EM_{LIN} is linear in the ensemble mean wave response, while the term EM_{NL} is

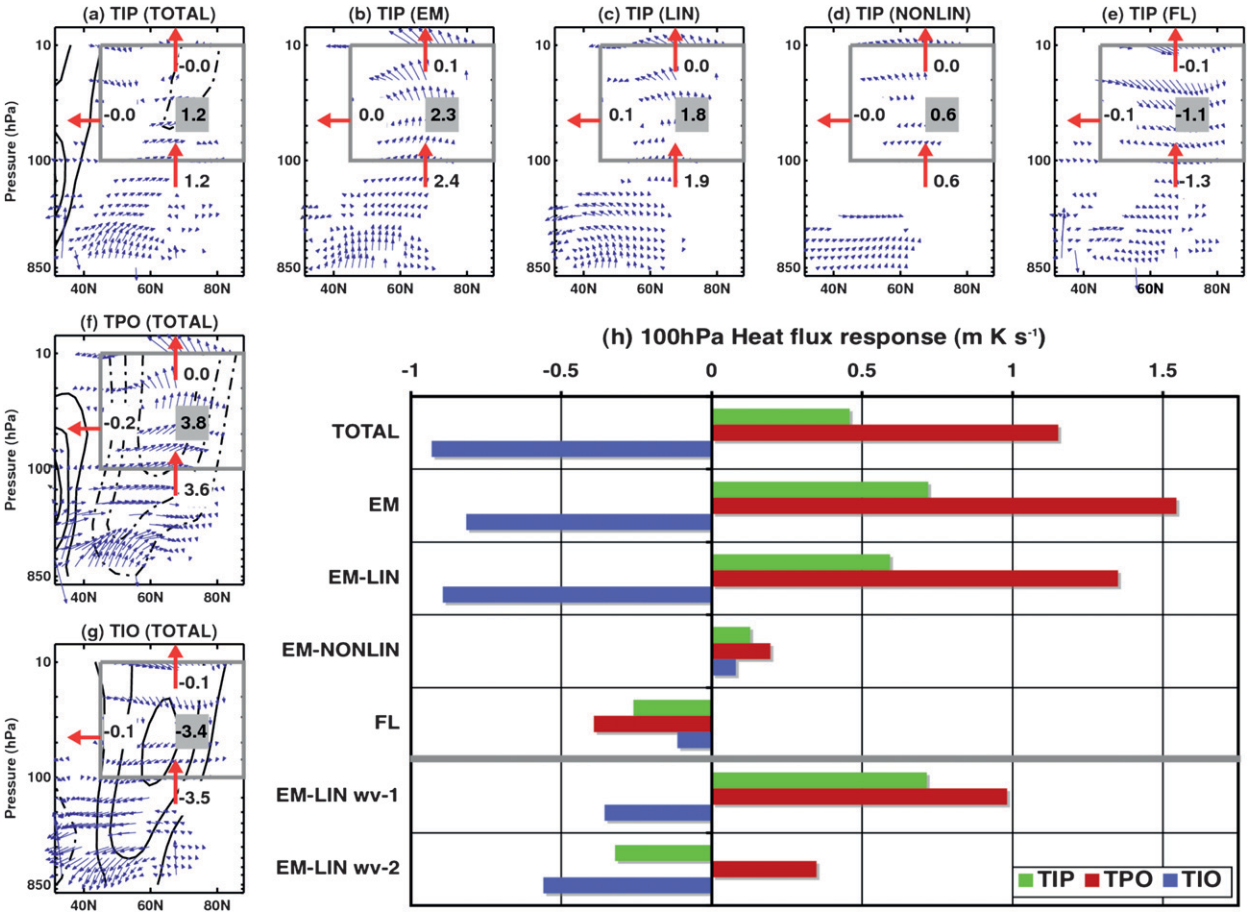

FIG. 6. (a)–(g) Results of the EP flux budget analysis computed for the gray boxes. Red arrows and numbers show fluxes through the box boundaries, while numbers in gray denote the response of the total EP flux convergence into the box (all numbers are in units of 10^4 kg m s^{-4}; see section 3b). Blue vectors show the EP flux divided by the basic-state density; the maximum horizontal (vertical) arrow length is 10 (0.25) $\times$ 10^6 kg s^{-2}. The three panels in the left column show the TOTAL EP flux response and budget for the TIP, TPO, and TIO simulations, and the response in the zonal mean zonal wind (contours: interval is 1 m s^{-1} and negative contours are dashed). (b)–(e) Individual terms from the EP flux decomposition following the analysis in section 3b. (h) The contribution to the total 100-hPa eddy meridional heat flux response ($\Delta\{\langle v^*T^*\rangle\}$) from the terms in the decomposition, averaged between 40° and 80°N.

quadratic in the ensemble mean wave response. The EM_{LIN} term represents the linear interference effect, which involves the phase difference between the wave response and the climatological wave. Furthermore, if wave responses are additive in the forcing (as was the case for TPO + TIO = TIP; see section 3a), then their respective EM_{LIN} terms should also be additive. The EM_{NL} term, by contrast, reflects the wave activity intrinsic to the wave response itself: the EM_{NL} wave activity flux (heat flux) term will be positive for upward-propagating Rossby waves and negative for downward-propagating Rossby waves, independent of the sign of the forcing or the phase of the wave. Additivity in the forcings will not in general be satisfied in EM_{NL}.

Although EM_{LIN} in (5) is linear in the wave response, this does not imply that the wave response itself is governed by linear dynamics. For example the wave response can typically involve nonlinear interactions among transient eddies, diabatic heating, orographic effects, etc. (Branstator 1992). We saw evidence of such nonlinearity in the Indian Ocean sector response (section 3a). The term ''linear'' applied to the decomposition here has a more specific meaning: given the wave response, the separate impacts on the zonal mean of terms that are linear and nonlinear in the wave response can be diagnosed. The intrinsic linearity or nonlinearity of the wave response is a separate issue that we will address in only a limited way in this study (section 4).

Following Hu and Tung (2002), we compute an EP flux budget for a box in the extratropical lower stratosphere that extends in latitude from 45° to 90°N and in pressure from 100 to 10 hPa (approximately 17–35 km). The integral of the EP flux divergence can be broken up

into four terms, each representing the flux through one side of the box. By examining the EP flux budget at high latitudes, we aim to determine the changes to the wave activity absorbed in the vicinity of the polar vortex. This will help explain the zonal mean NAM responses seen in Figs. 5a–c.

c. *Diagnosing the wave activity response*

In the left-hand column of Fig. 6, we present the EP flux and zonal wind response for the TIP, TPO, and TIO cases. As expected from the geopotential response in Fig. 5, TIP shows a weak easterly response in the extratropical zonal winds of the troposphere and stratosphere, TPO shows a strong easterly response, and TIO shows a strong westerly response. For the wave activity flux into the stratosphere, TIP shows a moderate increase in the flux, TPO shows a relatively large increase in the flux, and TIO shows a relatively large decrease in the flux. The TIP zonal wind response is approximately equal to the sum of the TPO and TIO responses (not shown), appearing as a residual of two responses that largely cancel. However, in the wave activity the responses are not additive: the sum of the TPO (Fig. 6f) and TIO (Fig. 6g) budgets is 0.4 units,[2] whereas the TIP budget (Fig. 6a) is 1.2 units. The relatively weak TIP response in both wind and wave activity therefore involves significant cancellation between the TPO and TIO cases, but the difference in wave activity flux convergence indicates that the response as a whole is not simply additive in the wave driving of these distinctively signed responses. The EP flux response fields in the TPO and TIO cases are in fact not equal and opposite, reflecting the distinct wave structures in the two cases. Thus, even if the net EP flux divergence is approximately equal and opposite, the connection between this value and the mean flow response might not be straightforward. We will here attempt to account for the most important differences between the extratropical TPO and TIO responses.

We now apply the decomposition described in section 3b to the EP flux response. Combining Eqs. (2) and (4),

$$\Delta\{\langle v^* T^* \rangle\} = \mathrm{TOTAL} = \mathrm{EM} + \mathrm{FL} \equiv \mathrm{EM}_{\mathrm{LIN}} + \mathrm{EM}_{\mathrm{NL}} + \mathrm{FL}.$$

In the top row of Fig. 6 we decompose the TOTAL EP flux response for TIP into these individual terms. These panels demonstrate that TOTAL is controlled by the EM term (Fig. 6b) rather than the FL term (Fig. 6e); that is, it is the ensemble mean wave activity response, rather than the response in the contribution from the fluctuations, that determines the TOTAL wave activity response. Specifically, the TOTAL, EM, and FL terms are +1.2, +2.3, and −1.1 in the units of the EP flux budget. Thus, $|\mathrm{EM}|/|\mathrm{FL}| \approx 2.1$. Furthermore, the EM term is dominated by the $\mathrm{EM}_{\mathrm{LIN}}$ component (Fig. 6c; $\mathrm{EM}_{\mathrm{LIN}}/\mathrm{EM} \approx +0.8$), which means that constructive interference between the response wave and the background wave dominates the EM wave activity response. In all the EP flux cross sections in Fig. 6, the total wave activity flux absorbed is almost completely dominated by the vertical flux into the bottom of the box—the term proportional to $\Delta\{\langle v^* T^* \rangle\}$—because the EP flux through the other sides of the box is relatively small. We thus use this term to represent the net EP flux into the stratosphere for the other cases.

The inset bar plot (Fig. 6h) shows the decomposition of the TOTAL $\Delta\{\langle v^* T^* \rangle\}$ response for TIP, TPO, and TIO. In all cases, EM is of larger magnitude than FL and $\mathrm{EM}_{\mathrm{LIN}}$ is the dominant contributor to EM. This is especially true of the TPO and TIO cases, where the net wave activity response is larger than TIP by a factor of 2–3. Thus, it is constructive or destructive interference between the ensemble mean and the climatological wave that characterizes the wave activity response as a whole. In particular, it is the change in sign of the linear term that accounts for the change in sign of the wave activity and, we infer, of the NAM response: in the TPO case, $\mathrm{EM}_{\mathrm{LIN}}$ is positive and in the TIO case $\mathrm{EM}_{\mathrm{LIN}}$ is negative.

The two nonlinear terms, $\mathrm{EM}_{\mathrm{NL}}$ and FL, are not negligible, but play less of a controlling role. The nonlinear terms are consistent in each of the three cases: the $\mathrm{EM}_{\mathrm{NL}}$ term is consistently positive and corresponds to enhanced upward wave activity flux, whereas the FL term is consistently negative and corresponds to reduced upward wave activity flux. We have a good understanding of why the $\mathrm{EM}_{\mathrm{NL}}$ term is positive (see below in this section) but a poorer understanding of why the FL term is consistently negative (see section 4). The cancellation between TPO and TIO in the TIP case causes the nonlinear terms to play a proportionally greater role, even if they are still relatively small compared to the linear term. Nonlinear and transient eddy effects in TIP might account for the nonadditivity in the EP fluxes noted above.

More insight into the EM flux response comes when we examine the climatological stationary wave and the ensemble mean response waves together. Figure 7, which plots the longitude–pressure cross section of waves 1 and 2 at 60°N, shows that TIP and TPO each produce a strong wave-1 response that is in phase with the background stationary wave. In contrast, in TIO both wave 1 *and wave 2* are strongly out of phase, giving

[2] The units of the integrated EP flux budget are kg m s^{-4}.

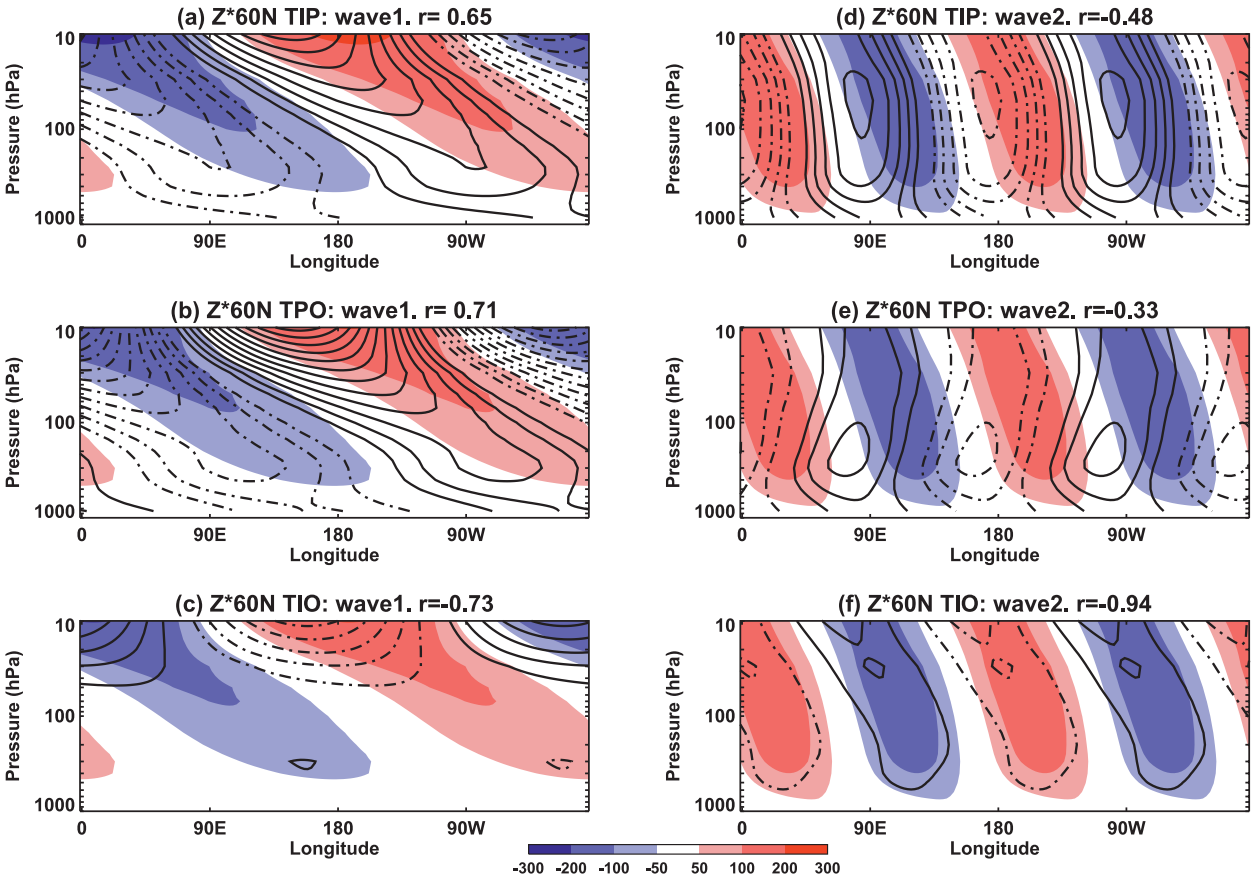

FIG. 7. Longitude–pressure sections of the ensemble-mean JF wave geopotential height at 60°N ($Z \times 60$N) in (a),(d) TIP, (b),(e) TPO, and (c),(f) TIO. Contours show the Z × 60N response (perturbed − control) (interval of 20 m; negative contours are dashed). Shading shows the climatological (stationary) wave field from the unforced control simulation.

further indication of why EM_{LIN} for TIO is opposite to EM_{LIN} for TPO and stronger than expected from the forcing strength. We quantify the spatial coherence between the background and response waves using the pressure-weighted anomaly correlation between the two fields. For TPO the wave-1 correlation is $r = 0.74$ compared to $r = -0.73$ for TIO; the correlations are nearly equal and opposite, consistent with the 180° shift in the wave-1 response (see also Figs. 4b and 4c). As might be expected from Figs. 4e and 4f, the situation is somewhat more complicated for wave 2. In the TPO case, the wave-2 response (Fig. 7e) is in approximate quadrature with the background wave in the troposphere and anticorrelated with the background wave in the stratosphere; it decays and tilts eastward with height. In contrast, in TIO the wave-2 response is even more strongly anticorrelated with the background wave than the wave-1 response (Fig. 7f; $r = -0.95$). Overall, the TIP wave response approximates a linear combination of the TPO and TIO responses for wave 1, but the responses are less additive in wave 2. These relationships are also evident in the bottom two rows of Fig. 6h, which decomposes the wave-1 and -2 contributions to EM_{LIN}. Figure 7 also shows that the wave responses generally exhibit a westward tilt with height, with the exception of wave 2 in TPO. Such a structure corresponds to an upward-propagating Rossby wave, and will contribute to a positive heat flux response. Thus, the westward tilt with height is reflected in the positive EM_{NL} response in all the cases seen in Fig. 6h.

We have taken the viewpoint that the tropospheric NAM is strongly coupled to the stratospheric NAM in these simulations. Thus, wave-driven impacts from the tropical SST perturbations on the extratropical stratospheric circulation are also expected to affect the troposphere. We see evidence of this in Figs. 5–6, which show that the zonal mean responses to the forcing extend from the troposphere into the stratosphere. The time-evolving response also involves strong stratosphere–troposphere coupling: when we examine the transient response to switch-on forcing in the TIO and TPO cases, we see that the zonal mean geopotential response begins in the

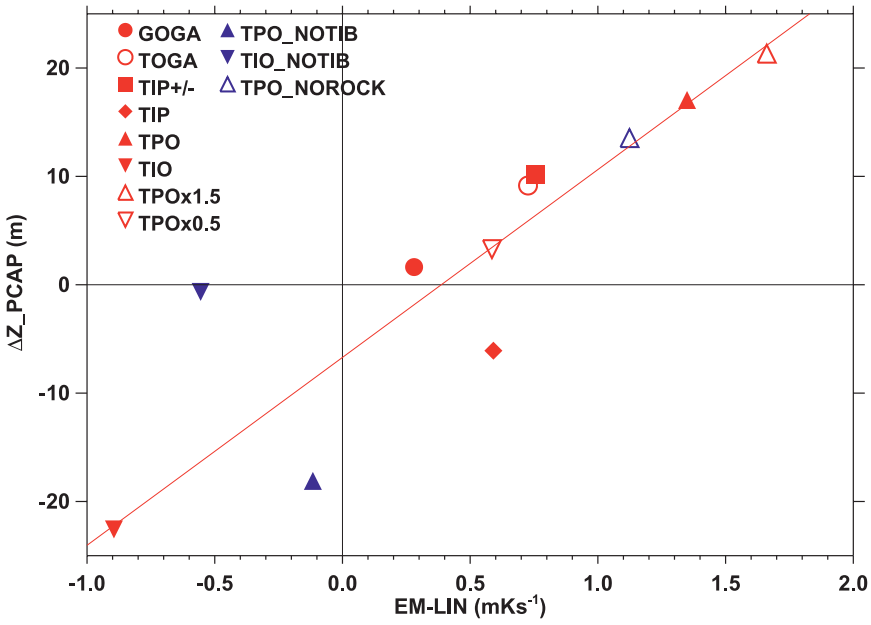

FIG. 8. Scatterplot showing the ensemble mean JF time-averaged response in the 100-hPa EM_{LIN} eddy meridional heat flux (v^*T^*, see section 3b for details) averaged between 40° and 80°N against the JF 850-hPa geopotential height response averaged over the polar cap north of 60°N (ΔZ_PCAP). The red symbols denote simulations conducted using the standard configuration of the model. The blue symbols denote simulations with perturbed topography and stationary waves; the suffix NOTIB (NOROCK) denotes a simulation where Eurasian (North American) topography is reduced to sea level (see Table 1 and section 3d for more details). The straight line is a least squares fit to the standard configuration cases (red symbols) only.

stratosphere then progresses down to the troposphere over a time scale of several weeks (not shown).

In Fig. 8 we establish a clearer link between the EM_{LIN} term and the tropospheric NAM response. On the basis of this figure and other more detailed analysis we argue that since (a) greater wave activity fluxes into the stratosphere are associated with stronger negative tropospheric NAM responses and (b) the wave activity flux response in these simulations is generally dominated by the linear interference term, then (c) a more positive EM_{LIN} term should be associated with a more negative tropospheric NAM response. Figure 8 includes results from the additional simulations listed in Table 1, with various forcings and climatological stationary wave fields. There is no guarantee that the wave activity flux–NAM response relationship should be the same for all cases, but many of the simulations fall on the same sensitivity line. Even in cases where the wave response exhibits nonlinearity in the amplitude of the response to the forcing, the sensitivity of the tropospheric NAM response per unit EM_{LIN} wave driving is similar. For example, comparing TPO × 0.5, TPO, and TPO × 1.5, for which the forcing varies in the ratio 1:2:3, the amplitude of the response varies nonlinearly with this forcing, but the three simulations fall along the same sensitivity line. The GOGA, TOGA, and TIP± simulations line up similarly.

The GOGA case is another weak-response case like TIP, but for reasons we do not fully understand the TIP case lies well below the best-fit line, which is estimated for the red symbols in Fig. 8. On the other hand, in the TIP± simulations, in which the observed positive and negative SST anomalies that are associated with ENSO are applied in the TIP region (Figs. 1a and 1b), we obtain a response that is very similar to the TOGA response. The NAM response in TIP± (not shown) also more closely resembles the response found in other models (Ineson and Scaife 2009; Cagnazzo and Manzini 2009) and the NAM pattern that is coherent with El Niño in observations (Garfinkel and Hartmann 2008). Other outliers are the two cases denoted NOTIB (see Table 1), for which the climatological stationary wave amplitude in the model has been artificially reduced, and linear interference effects are suppressed.

While the idea that tropical SST perturbations and extratropical surface climate may be connected through stratospheric wave–mean flow interaction is not new, our results include the following novel aspects: 1) the NAM response can be usefully decomposed into physically

distinct effects that are linear and nonlinear in the wave response, 2) the linear effects involve the coherence between the climatological wave and the wave response, 3) the nonlinear ensemble mean wave response corresponds consistently to upward-propagating wave activity, 4) there is a strong connection between the linear component of the EP flux entering the stratosphere and the NAM response in the troposphere, and 5) the transient eddy response is less predictable but typically not crucial for the NAM response. Thus, our main contribution is to present new diagnostics that clarify important aspects of the dynamics of this problem.

d. Sensitivity to perturbing the background waves

We have found that the NAM response to tropical warming is determined by EM_{LIN} and EM_{NL} contributions that depend in very different ways on the background climatological state and the forcing amplitude. We can use the atmospheric GCM framework to explore different regimes, even unrealistic ones, to test and improve our physical understanding of the NAM response. In this section, we reduce the amplitude of the background climatological stationary wave while keeping the TPO and TIO forcings fixed, with the expectation that this will reduce the relative importance of the linear interference on the NAM response.

We carry out a series of simulations, denoted NOTIB, in which we reduce the high topography over Tibet and eastern Eurasia to sea level. For each realization in the original TPO and TIO ensembles discussed in sections 3a–c (henceforth the standard cases), we run a new control and perturbation pair using identical SST forcings but with the reduced topography (henceforth TPO_{NOTIB} and TIO_{NOTIB}).[3] As expected, the NOTIB control simulation has a weaker background stationary wave and stronger polar vortex relative to the standard control simulation. The strengthening of the polar vortex is predominantly due to reduced planetary wave strength, as well as to a reduction in the strength of the parameterized lower-stratospheric orographic gravity wave drag.

The change in the stratosphere does not fundamentally alter the stratospheric wave propagation environment: the vortex is strengthened by about 30% and the winds throughout the NH remain below the Charney–Drazin critical velocity for Rossby wave propagation (not shown). As a result, the Rossby wave responses in the NOTIB simulations have similar spatial patterns to the standard cases but their amplitudes are 10%–20% stronger (not shown). In TIO_{NOTIB}, the wave refracts more equatorward than in the standard case (which was shown in Fig. 3c), suggesting that at least part of the difference in trajectory observed between TPO and TIO in the standard case is related to the proximity of the TIO to the Tibetan Plateau.

The amplitudes and spatial patterns of the wave response in the standard and NOTIB simulations are similar, which suggests that the dynamics governing the wave responses are independent of the stratospheric zonal flow and the climatological stationary wave. But the NAM response for this case (Figs. 9a and 9b) is much weaker than for the standard case (Figs. 5a and 5b). The heat flux decomposition (Fig. 9d, which should be compared to Fig. 6h) shows that the weak NAM response is explained by a weak TOTAL and EM response for both cases, which in turn is dominated by the EM_{LIN} component. Relative to the standard case, the EM_{LIN} term is attenuated more in TPO_{NOTIB} than TIO_{NOTIB} because 75% of the response in TPO comes from wave 1 (Fig. 6h), and wave 1 is weakened more in the NOTIB experiments than wave 2 (Fig. 9d bottom two rows); this is because Eurasian topography preferentially forces the climatological wave 1. The NOTIB simulations are more controlled by EM_{NL} and FL than the standard cases (Fig. 8), since the wave response is of larger amplitude than the climatological wave (not shown).

We also carried out a TPO warming experiment where the Rockies were reduced to sea level (TPO_{NOROCK}), but this has relatively little impact on wave 1, which dominates the TPO response. Thus, the high-latitude $[\Delta Z]$ (Fig. 9c) is weaker than in the standard case, but only by around 50%. Here, the weakening of the zonal response is caused by a combination of a reduction in EM_{LIN} through wave 2 and increased cancellation by the FL term (Fig. 9d). Thus, in addition to the large impacts on the NAM response from the location of tropical SST anomalies, we find that differences in regional topographic forcing also contribute significantly to the response through the climatological wave structure.

Finally, we note that the tropical–subtropical $[\Delta Z]$ is comparable in the standard experiments (Figs. 5a–c) and the corresponding sensitivity experiments NOTIB–NOROCK (Figs. 9a–c). This part of the response appears to be independent of the climatological wave structure and the location of the forcing, but it does scale roughly with forcing strength.

4. Discussion and conclusions

Using a set of atmospheric GCM simulations, we have investigated the zonal mean northern annular mode

[3] In our evaluation, it was not necessary to perform a NOTIB version of the TIP simulation because the changes related to topography are clearly explained through TPO_{NOTIB} and TIO_{NOTIB}.

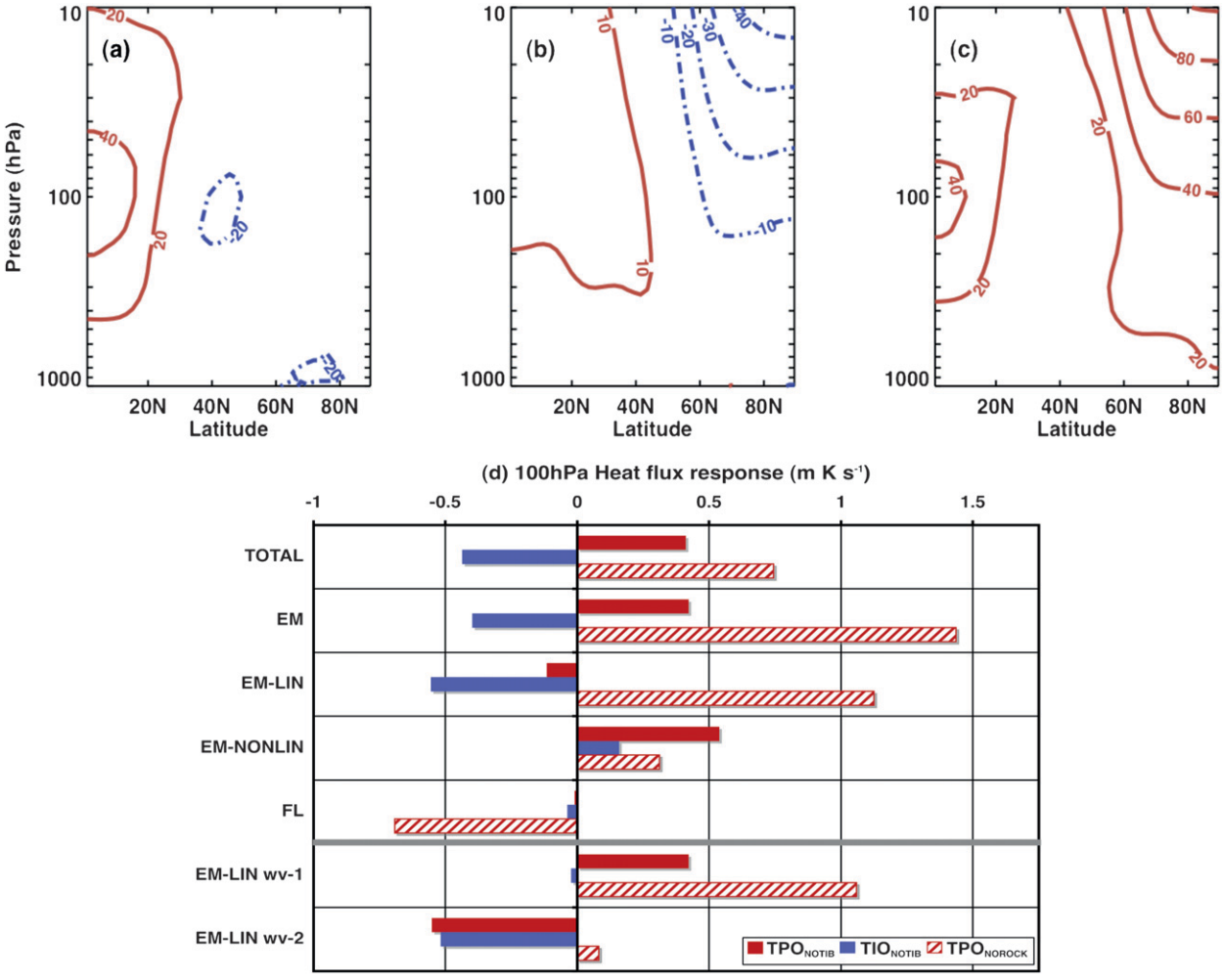

FIG. 9. The ensemble-mean JF zonal mean geopotential height response in (a) TPO_{NOTIB}, (b) TIO_{NOTIB} and (c) TPO_{NOROCK}. The inset bar plot in (d) is like Fig. 6h, but for the NOTIB and NOROCK simulations.

(NAM) response to imposed tropical Pacific (TPO) and Indian Ocean (TIO) SST warming. Imposing the TPO and TIO forcings together leads, in this model, to a weak positive NAM response consistent in sign with the ENSO–NAM connection that has been suggested in previous observational and modeling studies. The TPO and TIO forcings separately produce zonal mean NAM responses that are opposite and largely cancel, despite the TIO forcing being of the same sign and less than half the strength of TPO. We have shown that the zonal response is explained almost entirely by opposing linear interference of the response wave and climatological stationary waves in TPO and TIO. We also conducted a series of idealized simulations where the amplitude of the climatological stationary wave is weakened by reducing the model topography over Eurasia and North America. This attenuates the linear interference effect and significantly weakens the zonal response to tropical SST warming. Collectively, the results in section 3 highlight the importance for the NAM response on the phase and amplitude of the background stationary wave.

Our use of a linear interference diagnostic should not be taken to mean that the dynamics determining the wave response is simple or linear. Our sense is that the wave-1 responses are more predictable, robust, and linear than the wave-2 responses, and that a detailed study of the wave-2 response might prove useful. For example, Figs. 4e and 4f show significant phase and amplitude sensitivity in wave 2 that cannot be simply related to forcing strength or location. To make progress, it might be necessary to use a more idealized forcing. To properly compare TPO and TIO heating effects, a cleaner approach might be to assess the teleconnection response associated with imposed uniform SST warming ''patches'' at different locations in the tropics (e.g., Barsugli et al. 2006). Furthermore, since the actual forcing on the atmosphere comes not

from SST directly but through convective heating, future simulations should explicitly prescribe the free-tropospheric heat source as a forcing term on the thermodynamic equation (e.g., Branstator and Haupt 1998).

Our understanding of the FL contribution to the wave activity response discussed in sections 3c and 3d is rudimentary. In the upper troposphere and stratosphere they likely represent intermittent wave activity pulse events; a negative response in this term indicates that these events are reduced in strength, frequency, or both strength and frequency. There is also a significant FL response in the troposphere in these simulations, which could relate to synoptic eddy-driving adjustments in response to the tropical heating. These terms are generally unpredictable. For example, we note without explanation that TPO warming produced a disproportionately large FL response compared to TIO (Fig. 6h). The transient eddies are controlled both by the zonal mean and the zonally asymmetric climatological flow, as well as topographic forcing, and their stratospheric component might not be realistically represented in this model, which has relatively coarse vertical resolution. Furthermore, the FL term could reflect nonlinear aspects of the ensemble mean wave response that we have not considered, since synoptic transients likely maintain the ensemble mean (EM) wave response (Shutts 1983).

We are interested in which aspects of our results apply more generally, and which aspects are specific to the GFDL AM2 model. Several previous studies have highlighted the need to use multimodel ensembles in order to obtain robust teleconnection signals (e.g., Hoerling and Kumar 2002, 2004; Annamalai et al. 2007). We have identified three key areas that could exhibit model dependence from our results: (a) the tropical heating response to imposed SST anomalies is likely to be sensitive to model resolution and convective parameterizations; (b) different models have very different background stationary waves (Brandefelt and Körnich 2008), which we have shown in section 3d could have significant impacts on teleconnections; and, (c) the absence of a well-resolved stratospheric circulation in GFDL AM2 could influence wave–mean flow interactions and stratosphere–troposphere coupling (Cagnazzo and Manzini 2009; Bell et al. 2009). To test these other features of the response, we are currently producing a set of simulations with a second atmospheric GCM using the same forcing patterns but with different horizontal and vertical resolutions. Feedbacks between the atmosphere and the oceans, neglected in our simulations, have also been shown to influence the high-latitude circulation response (e.g., Li et al. 2006), and to fundamentally change the model basic state (Newman et al. 2009 and references therein); future work must therefore investigate the impacts on our results from coupling to an ocean.

Internal variability could lead to a lack of robustness that obscures the ENSO–NAM link. For example, while all of our plotted results are robust, it requires at least 30 realizations before we converge to a robust high-latitude NAM response. Furthermore, it is likely that part of the NAM variability associated with ENSO in observations is controlled by other processes, for example, the phase of the quasi-biennial oscillation (Camp and Tung 2007; Garfinkel and Hartmann 2008), and by solar modulation (Kryjov and Park 2007), which we have not considered.

We would like to reiterate that it remains uncertain whether Indian Ocean SST anomalies can play an active role in generating convective heating anomalies that initiate teleconnections. The Indian Ocean SST warming that was imposed in our TIO simulations is known to be driven, at least in part, by the atmospheric response to warm ENSO events in the tropical Pacific (Alexander et al. 2002). Furthermore, recent warming trends in the Indian Ocean, which in modeling studies has been shown to force decadal and multidecadal trends in the North Atlantic Oscillation (Hoerling et al. 2004; Bader and Latif 2005), may also be driven by the atmosphere (Copsey et al. 2006). It is beyond the scope of this study to assess what causes the Indian Ocean to warm, or how tropical–extratropical teleconnections forced from the Pacific and the Indian Ocean may interact on longer time scales. However, these issues are likely to be important when considering the impacts of anthropogenic climate change on future ENSO teleconnections.

Finally, we believe that these results offer the prospect of improving seasonal prediction systems for the northern extratropics by combining information about the location of tropical SST anomalies and the climatological stationary wave to improve forecasts of the NAM index and, therefore, weather patterns over large areas of western Europe and North America. For example, model predictions of El Niño teleconnections could be weighted by the magnitude of SST anomalies in other basins, particularly the Indian Ocean. Our results highlight the importance for seasonal prediction models to accurately simulate both the atmospheric response to tropical heating, and also the climatological stationary wave structure.

Acknowledgments. We acknowledge support from Canadian Foundation for Climate and Atmospheric Sciences Grant 506, the National Oceanic and Atmospheric Administration's Geophysical Fluid Dynamics Laboratory. L for the model code, and the Canadian Institute for Theoretical Astrophysics for the computer

resources. We thank the reviewers for their helpful comments.

REFERENCES

Alexander, M. A., I. Blade, M. Newman, J. R. Lanzante, N. C. Lau, and J. D. Scott, 2002: The atmospheric bridge: The influence of ENSO teleconnections on air–sea interaction over the global oceans. *J. Climate,* **15,** 2205–2231.

Anderson, J., and Coauthors, 2004: The new GFDL Global Atmosphere and Land Model AM2–LM2: Evaluation with prescribed SST simulations. *J. Climate,* **17,** 4641–4673.

Annamalai, H., H. Okajima, and M. Watanabe, 2007: Possible impact of the Indian Ocean SST on the Northern Hemisphere circulation during El Niño. *J. Climate,* **20,** 3164–3189.

Bader, J., and M. Latif, 2005: North Atlantic Oscillation response to anomalous Indian Ocean SST in a coupled GCM. *J. Climate,* **18,** 5382–5389.

Baldwin, M. P., and T. P. Dunkerton, 2001: Stratospheric harbingers of anomalous weather regimes. *Science,* **294,** 581–584.

——, and D. W. J. Thompson, 2009: A critical comparison of stratosphere–troposphere coupling indices. *Quart. J. Roy. Meteor. Soc.,* **135,** 1661–1672.

Barsugli, J. J., and P. D. Sardeshmukh, 2002: Global atmospheric sensitivity to tropical SST anomalies throughout the Indo-Pacific basin. *J. Climate,* **15,** 3427–3442.

——, S. I. Shin, and P. D. Sardeshmukh, 2006: Sensitivity of global warming to the pattern of tropical ocean warming. *Climate Dyn.,* **27,** 483–492.

Bell, C. J., L. J. Gray, A. J. Charlton-Perez, M. M. Joshi, and A. A. Scaife, 2009: Stratospheric communication of El Niño teleconnections to European winter. *J. Climate,* **22,** 4083–4096.

Brandefelt, J., and H. Körnich, 2008: Northern Hemisphere stationary waves in future climate projections. *J. Climate,* **21,** 6341–6353.

Branstator, G., 1992: The maintenance of low-frequency atmospheric anomalies. *J. Atmos. Sci.,* **49,** 1924–1945.

——, and S. E. Haupt, 1998: An empirical model of barotropic atmospheric dynamics and its response to tropical forcing. *J. Climate,* **11,** 2645–2667.

Brönnimann, S., 2007: Impact of El Niño–Southern Oscillation on European climate. *Rev. Geophys.,* **45,** RG3003, doi:10.1029/2006RG000199.

Cagnazzo, C., and E. Manzini, 2009: Impact of the stratosphere on the winter tropospheric teleconnections between ENSO and the North Atlantic and European region. *J. Climate,* **22,** 1223–1238.

Camp, C. D., and K. K. Tung, 2007: Stratospheric polar warming by ENSO in winter: A statistical study. *Geophys. Res. Lett.,* **34,** L04809, doi:10.1029/2006GL028521.

Cohen, J., D. Salstein, and K. Saito, 2002: A dynamical framework to understand and predict the major Northern Hemisphere mode. *Geophys. Res. Lett.,* **29,** 1412, doi:10.1029/2001GL014117.

Copsey, D., R. Sutton, and J. R. Knight, 2006: Recent trends in sea level pressure in the Indian Ocean region. *Geophys. Res. Lett.,* **33,** L19712, doi:10.1029/2006GL027175.

Delworth, T. L., and Coauthors, 2006: GFDL's CM2 global coupled climate models. Part I: Formulation and simulation characteristics. *J. Climate,* **19,** 643–674.

Fletcher, C. G., S. C. Hardiman, P. J. Kushner, and J. Cohen, 2009: The dynamical response to snow cover perturbations in a large ensemble of atmospheric GCM integrations. *J. Climate,* **22,** 1208–1222.

Free, M., and D. J. Seidel, 2009: Observed El Niño–Southern Oscillation temperature signal in the stratosphere. *J. Geophys. Res.,* **114,** D23108, doi:10.1029/2009JD012420.

Garfinkel, C. I., and D. L. Hartmann, 2008: Different ENSO teleconnections and their effects on the stratospheric polar vortex. *J. Geophys. Res.,* **113,** D18114, doi:10.1029/2008JD009920.

Gill, A. E., 1980: Some simple solutions for heat-induced tropical circulation. *Quart. J. Roy. Meteor. Soc.,* **106,** 447–462.

Hoerling, M. P., and A. Kumar, 2002: Atmospheric response patterns associated with tropical forcing. *J. Climate,* **15,** 2184–2203.

——, J. W. Hurrell, T. Xu, G. T. Bates, and A. S. Phillips, 2004: Twentieth century North Atlantic climate change. Part II: Understanding the effect of Indian Ocean warming. *Climate Dyn.,* **23,** 391–405.

Horel, J. D., and J. M. Wallace, 1981: Planetary-scale atmospheric phenomena associated with the Southern Oscillation. *Mon. Wea. Rev.,* **109,** 813–829.

Hu, Y. Y., and K. K. Tung, 2002: Interannual and decadal variations of planetary wave activity, stratospheric cooling, and Northern Hemisphere Annular mode. *J. Climate,* **15,** 1659–1673.

Ineson, S., and A. A. Scaife, 2009: The role of the stratosphere in the European climate response to El Niño. *Nat. Geosci.,* **2,** 32–36.

Kryjov, V. N., and C. K. Park, 2007: Solar modulation of the El-Niño/Southern Oscillation impact on the Northern Hemisphere annular mode. *Geophys. Res. Lett.,* **34,** L10701, doi:10.1029/2006GL028015.

Kumar, A., and M. P. Hoerling, 1998: Specification of regional sea surface temperatures in atmospheric general circulation model simulations. *J. Geophys. Res.,* **103,** 8901–8907.

Li, S. L., M. P. Hoerling, S. L. Peng, and K. M. Weickmann, 2006: The annular response to tropical Pacific SST forcing. *J. Climate,* **19,** 1802–1819.

Lin, S. J., 2004: A ''vertically Lagrangian'' finite-volume dynamical core for global models. *Mon. Wea. Rev.,* **132,** 2293–2307.

Manzini, E., 2009: Atmospheric science: ENSO and the stratosphere. *Nat. Geosci.,* **2,** 749–750, doi:10.1038/ngeo677.

——, M. A. Giorgetta, M. Esch, L. Kornblueh, and E. Roeckner, 2006: The influence of sea surface temperatures on the northern winter stratosphere: Ensemble simulations with the MAECHAM5 model. *J. Climate,* **19,** 3863–3881.

Newman, M., P. D. Sardeshmukh, and C. Penland, 2009: How important is air–sea coupling in ENSO and MJO evolution? *J. Climate,* **22,** 2958–2977.

Newman, P. A., E. R. Nash, and J. E. Rosenfield, 2001: What controls the temperature of the Arctic stratosphere during the spring? *J. Geophys. Res.,* **106** (D17), 19 999–20 010.

Polvani, L. M., and D. W. Waugh, 2004: Upward wave activity flux as a precursor to extreme stratospheric events and subsequent anomalous surface weather regimes. *J. Climate,* **17,** 3548–3554.

Rayner, N. A., D. E. Parker, E. B. Horton, C. K. Folland, L. V. Alexander, D. P. Rowell, E. C. Kent, and A. Kaplan, 2003: Global analyses of sea surface temperature, sea ice, and night marine air temperature since the late nineteenth century. *J. Geophys. Res.,* **108,** 4407, doi:10.1029/2002JD002670.

Shutts, G. J., 1983: The propagation of eddies in diffluent jetstreams: Eddy vorticity forcing of 'blocking' flow fields. *Quart. J. Roy. Meteor. Soc.,* **109,** 737–761.

Smith, K. L., C. G. Fletcher, and P. J. Kushner, 2010: The role of linear interference in the annular mode response to extratropical surface forcing. *J. Climate,* **23,** 6036–6050.

Thompson, D., and J. Wallace, 2000: Annular modes in the extratropical circulation. Part I: Month-to-month variability. *J. Climate,* **13,** 1000–1016.

Trenberth, K. E., G. W. Branstator, D. Karoly, A. Kumar, N. C. Lau, and C. Ropelewski, 1998: Progress during TOGA in understanding and modeling global teleconnections associated with tropical sea surface temperatures. *J. Geophys. Res.,* **103** (C7), 14 291–14 324.

Wallace, J. M., and D. S. Gutzler, 1981: Teleconnections in the geopotential height field during the Northern Hemisphere winter. *Mon. Wea. Rev.,* **109,** 784–812.

Wilks, D. S., 2006: *Statistical Methods in the Atmospheric Sciences*. Academic Press, 648 pp.

Wu, R. G., B. P. Kirtman, and K. Pegion, 2006: Local air–sea relationship in observations and model simulations. *J. Climate,* **19,** 4914–4932.